Biogeosciences Discuss., 10, 2937–2965, 2013
www.biogeosciences-discuss.net/10/2937/2013/
doi:10.5194/bgd-10-2937-2013

Biogeosciences Discussions Open Access

Regional variability of acidification in the Arctic: a sea of contrasts

E. E. Popova, A. Yool, A. C. Coward, and T. R. Anderson

National Oceanography Centre, University of Southampton Waterfront Campus, European Way, Southampton SO14 3ZH, UK

Received: 29 January 2013 – Accepted: 30 January 2013 – Published: 18 February 2013

Correspondence to: E. E. Popova (ekp@noc.ac.uk)

Published by Copernicus Publications on behalf of the European Geosciences Union.

Abstract

The Arctic Ocean is a region that is particularly vulnerable to the impact of ocean acidification driven by rising atmospheric CO_2, negatively impacting calcifying organisms such as coccolithophorids and foraminiferans. In this study, we use an ocean general circulation model, with embedded biogeochemistry and a full description of the carbon cycle, to study the response of pH and saturation states of calcite and aragonite to changing climate in the Arctic Ocean. Particular attention is paid to the strong regional variability within the Arctic and, for comparison, simulation results are contrasted with those for the global ocean. Simulations were run to year 2099 using the RCP 8.5 (the highest IPCC AR5 CO_2 emission scenario). The separate impacts of the direct increase in atmospheric CO_2 and indirect effects via climate feedbacks (changing temperature, stratification, primary production and fresh water fluxes) were examined by undertaking two simulations, one with the full system and the other in which ocean-atmosphera exchange of CO_2 was prevented from increasing beyond the flux calculated for year 2000. Results indicate that climate feedbacks, and spatial heterogeneity thereof, play a strong role in the declines in pH and carbonate saturation (Ω) seen in the Arctic. The central Arctic, Canadian Arctic Archipelago and Baffin Bay show greatest rates of acidification and Ω decline as a result of melting sea ice. In contrast, areas affected by Atlantic inflow including the Greenland Sea and outer shelves of the Barents, Kara and Laptev seas, had minimal decreases in pH and Ω because weakening stratification associated with diminishing ice cover led to greater mixing and primary production. As a consequence, the predicted onset of undersaturation is highly variable regionally within the Arctic, occurring during the decade of 2000–2010 in the Siberian shelves and Canadian Arctic Archipelago, but as late as the 2080s in the Barents and Norwegian Seas. We conclude that, in order to make future projections of acidification and carbon saturation state in the Arctic, regional variability needs to be adequately resolved, with particular emphasis on reliable predictions of the rates of retreat of the sea-ice which are a major source of uncertainty.

BGD
10, 2937–2965, 2013

1 Introduction

The concentration of CO_2 has been steadily rising in the atmosphere as a result of the burning of fossil fuels, cement manufacture and land-use changes (Friedlingstein et al., 2010). Further increases are expected on the basis of current emission rates, e.g. to 450–650 ppm by the mid-21st-century (Houghton et al., 2001). The ocean acts as a sink for this atmospheric carbon, with uptake estimated at 120–140 Pg C since preindustrial times (Sabine et al., 2004; Khatiwala et al., 2009). The invasion of CO_2 into the ocean has two important consequences for seawater chemistry, namely that both pH and carbonate saturation state (Ω) decrease. The ocean biota, and especially calcifying organisms such as coccolithophores, foraminiferans and pteropods, are particularly vulnerable to these changes (Fabry et al., 2008; Gangstøet al., 2011).

In addition to the direct impact of CO_2 invading the ocean, pH and saturation state are influenced by other aspects of changing climate including temperature increase, changes in ocean stratification (including associated changes in the net primary production), retreating sea-ice and increasing freshwater input. A number of studies have examined the relative importance of the direct impact of invading CO_2 and these other climate-related factors for the pH and Ω in the global ocean. McNeil and Matear (2007) remarked that temperature was the most important of the climate change factors. It has relatively little effect on pH because, although increasing temperature causes pH to decrease, it also buffers dissolved inorganic carbon (CT) increase (and associated pH decrease) through the reduction in CO_2 solubility. In contrast, carbonate saturation state, which is relatively insensitive to the direct effect of temperature, declines significantly because of increasing CT in the ocean, despite the buffering effect of temperature. The implication is that future projections of surface ocean acidification (pH) in the global ocean need only consider the direct effect of CO_2 invading the ocean, whereas the temperature effect is more relevant regarding carbonate saturation state.

The Arctic is an area that is particularly sensitive to changing climate (Walsh et al., 2011) as a result of so-called polar amplification (Moritz et al., 2002). Observations

BGD
10, 2937–2965, 2013

have shown that a number of areas in the Arctic Ocean are already undersaturated with respect to aragonite (e.g. the Canada Basin: Yamamoto-Kawai et al., 2009; freshwater-influenced shelves: Chierici and Fransson, 2009; the Chukchi, Beaufort and eastern East Siberian Seas: Bates et al., 2011). A number of modelling and observational studies have indicated that the Arctic Ocean, with its low temperatures, substantial fresh water input and fast retreating sea-ice, is a region where the impact of ocean acidification is likely to manifest itself first (McNeil and Matear, 2007; Yamamoto-Kawai et al., 2009; Yamamoto et al., 2012, Steinacher et al., 2009; Bates et al., 2011). Future declines in pH and Ω have been shown to closely track changes in atmospheric CO_2. The equilibration between oceanic and atmospheric CO_2 follows the well-established carbonate chemistry of sea-water, with only a relatively minor impact by the changing ocean physics in nearly all ocean regions except for the Arctic Ocean (e.g. Yamamoto et al., 2012; McNeil and Matear, 2007). The fast retreat of sea-ice leads to the exposure of previously undersaturated (with respect to CO_2) areas to the atmosphere, accelerating its absorption by the ocean. Other potential impacts include changes in stratification with consequences for nutrient supply and primary productivity (e.g. Popova et al., 2010), and the effect of freshwater input (Chierici and Fransson, 2009).

Various climate-related impacts on ocean acidification have been included in modelling studies, and have indicated that the Arctic Ocean will become undersaturated with respect to aragonite by the 2040s (e.g. Steinacher et al., 2009; Yamamoto et al., 2012). These studies generally assessed the impact of acidification in Arctic on the basis of basin-averaged or zonal characteristics. The Arctic Ocean is, however, an area with large spatial gradients in physical and biological properties (e.g. Carmack et al., 2006; Popova et al., 2010) and, even more importantly, it is an area where climate change factors are expected to have strong regional variations. In this paper we focus on regional aspects of Arctic Ocean acidification, with two main aims. First, using a global ocean general circulation model (GCM), we investigate the direct (invasion of CO_2) and indirect (climate-related) effects of increasing atmospheric CO_2 (changes in temperature, stratification, sea-ice cover and freshwater input) on pH and saturation

BGD
10, 2937–2965, 2013

state in the Arctic Ocean, undertaking an intercomparison with the rest of the global ocean. The GCM includes a full representation of the carbon cycle and is forced by the RCP 8.5 scenario (Jones et al., 2011) through the period 1860–2099. This run is described and analysed in detail for the global ocean by Yool et al. (2013b). The second aim is to study the heterogeneity of acidification and carbonate saturation state in the Arctic as predicted by the model, and to relate it to the variability in underlying factors. The direct and indirect effects are distinguished by comparing two parallel simulations of the model. The first run is that described above, where the ocean carbon system experiences both increasing atmospheric CO_2 and the resulting climate impacts on ocean physics and biology. The second simulation separates CO_2 and climate by holding atmospheric CO_2 constant at the year 2000 value while continuing to allow climate change.

2 Method

The Nucleus for European Modelling of the Ocean (NEMO) model is comprised of an ocean general circulation model, OPA (Madec, 2008), coupled with the Louvain-la-Neuve Ice Model v2, LIM2 (Timmermann et al., 2005). NEMO version 3.2 is used here which has a horizontal resolution of 1° and a vertical resolution of 64 levels achieving resolution of 5 m in the top 20 m of the water column. Vertical mixing is parameterised using the turbulent kinetic energy scheme of Gaspar et al. (1990). NEMO is forced by the output from a simulation of the HadGEM2-ES Earth system model run by the UK Meteorological Office (UKMO) that includes representations of the terrestrial and oceanic carbon cycles, atmospheric chemistry and aerosols (Collins et al., 2011). The HadGEM2-ES simulation used here, identifier AJKKH, was performed as part of the UKMO's input (Jones et al., 2011) to the Coupled Model Intercomparison Project 5 (CMIP5) and Assessment Report 5 (AR5) of the Intergovernmental Panel on Climate Change (IPCC). The frequency of output fields is monthly for precipitation (rain, snow,

BGD
10, 2937–2965, 2013

runoff), daily for radiation (downwelling short- and long-wave) and 6-hourly for the turbulent variables (air temperature, humidity and wind velocities).

Biogeochemistry in NEMO is represented by the plankton ecosystem model MEDUSA (Model of Ecosystem Dynamics, carbon Utilisation, Sequestration and Acidification; Yool et al., 2011, 2013a). This is a size-based, intermediate complexity model that divides the plankton community into "small" and "large" portions and which resolves the elemental cycles of nitrogen, silicon and iron. The "small" portion of the ecosystem is intended to represent the microbial loop of picophytoplankton and microzooplankton while the "large" portion covers microphytoplankton (specifically diatoms) and mesozooplankton. The intention of MEDUSA is to separately represent small, fast-growing phytoplankton that are kept in check by similarly fast-growing protistan zooplankton and large, slower-growing phytoplankton that are able to temporarily escape the control of slower-growing metazoan zooplankton. The non-living particulate detritus pool is similarly split between small, slow-sinking particles that are simulated explicitly, and large fast-sinking particles that are represented only implicitly. See Yool et al. (2013a) for a full description of the models.

Model performance with respect to ecosystem dynamics of the present day Arctic Ocean was assessed by Popova et al. (2010) and Popova et al. (2012) and globally by Yool et al. (2011). Model performance with respect to the global ocean carbon cycle is described in Yool et al. (2013a) and Yool et al. (2013b). For the Arctic Ocean we note good agreement of modelled values of surface saturation with respect to calcite (Ω_c), and aragonite (Ω_a) with values reported by Jutterström and Anderson (2005) for the central Arctic Ocean (1.9–2.7 for Ω_c and 1.1–1.8 for Ω_a measured during 1990s). Over the shelves of the Western Arctic Ocean and Baffin Bay the modelled values are in the same range as observations reported by Chierici and Fransson (2009) (8.0–8.2 for pH_{SWS},where SWS denotes sea water scale units; 1.8–3.0 for Ω_c 1.8–2.), however we note that the model underestimates high values of Ω_c and Ω_a in the Chukchi Sea (4 and 2.5 as reported by Chierici and Fransson, 2009 and Bates et al., 2012) by about 1 unit.

BGD
10, 2937–2965, 2013

3 Results

3.1 Regional aspects of Arctic Ocean acidification

Under the RCP 8.5 scenario, atmospheric CO_2 in the model reaches 950 ppm by the end of the century while globally averaged SST (sea surface temperature) rises from 18 to 22 °C (Fig. 1a, b). This increase is more pronounced in the Arctic Ocean (defined here as north of 66° N) due to polar amplification (Moritz et al., 2002) with SST changing from −1 to 4.5 °C (Fig. 1b). The associated decline of sea-ice leads to virtually ice-free conditions in summer in the Arctic Ocean from the 2060s onwards (Fig. 1c).

Ice retreat is the factor that most strongly influences the spatial distribution of the predicted declines of pH_{SWS} and Ω in the Arctic Ocean (e.g. McNeil and Matear, 2007). This is a result of increasing ocean uptake of CO_2, freshening of the surface layers by melt of the perennial ice and the weakening of stratification. Modelled annual mean sea-ice concentration for years 2000 and 2099 is shown in Fig. 2a, b. Seasonally ice-free conditions in the Arctic Ocean occur during the decade of the 2060s. By the end of the 21st century, the central Arctic Ocean becomes nearly ice-free on an annual basis and winter ice occurs only on the Siberian and Canadian shelves, including Baffin Bay (Fig. 2b). The retreat of the ice brings substantial changes to predicted surface salinity (Fig. 3a, b), with a strong decline over the shelves of the western Arctic Ocean and in Baffin Bay of up to 3 driven by the accumulation of the melt water. The second major area of salinity decline is the Siberian shelves (up to 4 due to the increase in riverine input). In the areas which change from being permanently ice-covered to permanently ice-free (the central Arctic Ocean), surface salinity increases by about 3–4. In addition, an increase in surface salinity occurs in areas of weakening of the stratification, mostly associated with Atlantic inflow (Fig. 3c, d).

We chose the maximum annual depth of the upper mixed layer (based on monthly mean values) as a convenient measure of the state of water column stratification. This is important as regards ecosystem functioning and the rate of acidification as it controls exchange with deeper layers with high salinity, temperature, nutrients, CT and low Ω.

BGD
10, 2937–2965, 2013

Stratification weakens over the majority of the Arctic Ocean (Fig. 3c, d), with the exception of the Norwegian and Western Barents Seas where ocean warming induces strong stabilisation of stratification, with shallowing of the winter mixing by more than 200 m. The strongest weakening of stratification occurs in areas of increased Atlantic inflow into the Arctic Ocean, namely the Greenland Sea and the outer shelves of the Barents, Kara and Laptev Seas, where deep mixing by the end of the century penetrates to 200–300 m.

The areas experiencing the largest changes in ice regime (from permanent ice cover as it is today to a year-round ice-free zone by 2099) and substantial freshening show the largest decreases in pH_{SWS} from 8.2 to 7.65 (Central Arctic Ocean, Canadian Arctic Archipelago and Baffin Bay, Fig. 4a, b), Ω_c from 2 to 1 (Fig. 4e, f) and Ω_a from 1.2 to 0.5 (Fig. 4i, j). The largest increase in CT is also seen in the central AO (Fig. 4m, n) due to equilibration with the atmosphere following the loss of permanent ice cover and an increase in vertical mixing. More than half of this increase (150 out of 220 mmol m^{-3}) happens as a result of climate feedbacks driving retreat of the ice, while only about 30–40 % of this increase is driven by rising CO_2 (Fig. 4o, p). Nevertheless, the area of maximum increase in CT does not correspond exactly to the area of maximum decline in pH_{SWS} and Ω. This is a consequence of the role of freshening as a factor in accelerating the decline of both pH_{SWS} and Ω, and plays a major role in the Canadian Arctic Archipelago and Baffin Bay.

In the case of Ω_c and Ω_a, the buffering effect of climate change is driven by changes in stratification (cf. Fig. 4h, l, d) and is strongest in the area of Atlantic inflow in the Greenland, northern Barents and Kara Seas. Substantial deepening of the winter mixing in these areas dilutes undersaturated surface waters reducing the impact of changes at the surface. In contrast, the stabilisation of stratification along the Norwegian Shelf does not appear to have a pronounced effect.

Relative to the acidification rates in the central Arctic Ocean and Canadian Arctic Archipelago, changes over the Siberian shelves occur more slowly (Fig. 4a–d). However, by 2099 values of pH_{SWS} and Ω are lower than those in the central Arctic Ocean

BGD
10, 2937–2965, 2013

since present day pH_{SWS} and Ω are already low in this area. Thus, by 2099 surface pH_{SWS} is as low as 7.6, while typical values of Ω_c and Ω_a are 0.8 and 0.4 respectively.

Values of pH_{SWS} and Ω decline more slowly over the Siberian, Beaufort and Chukchi shelves reflecting the opposite effect of climate change on these characteristics compared to the central Arctic and Canadian Arctic Archipelago. Today, these areas experience a substantial ice-free period during the year and so ocean CO_2 is well-equilibrated with the atmosphere. Thus, a more prolonged ice-free season does not impact CT concentration to the same extent as in the present permanently ice-covered areas. The climate change simulation shows a decline in CT in these areas by the end of the century (Fig. 4o). The main climate factor driving this decline appears to be the near doubling of the net primary production over the Chukchi, Beaufort and East Siberian shelves (Fig. 4f) and an increase of riverine inputs over the Siberian shelves. While the increase in the net primary production tends to increase pH_{SWS} and Ω by decreasing CT concentration, the increase in riverine freshwater inputs has the opposite effect. The two factors nearly cancel each other out (Fig. 4d, h, l) so that climate related factors have little impact on pH_{SWS} and Ω.

In summary, these results indicate that climate change feedbacks have a pronounced impact on pH_{SWS} and Ω in the Arctic Ocean in some areas, increasing (by up to factor of 2) their decline as driven by the rising of the atmospheric CO_2. In other areas buffering (for Ω) has little or no total impact. Thus, processes driven by climate change feedbacks create strong gradients in the rates of decline of pH_{SWS} and Ω across the basin.

3.2 Timing of the first occurrence of undersaturation conditions in the Arctic Ocean

By 2099, the model predicts that surface waters of the Arctic Ocean will be undersaturated with respect to aragonite in all areas (Fig. 4j). Some areas, however, escape undersaturation with respect to calcite, including the areas of the Arctic Ocean affected by Atlantic inflow: Greenland, Norwegian and Barents seas and the outer shelves of Kara Sea (Fig. 4f). As such, it is crucial to correctly estimate the time of the onset of

BGD
10, 2937–2965, 2013

undersaturation. The year of first occurrence of monthly mean undersaturated surface waters with respect to calcite and aragonite under the RCP 8.5 scenario is shown in Fig. 5a, b, while the same characteristic for shelf bottom waters is shown in Fig. 5c, d. With respect to aragonite, undersaturation of both surface and bottom waters is already widespread at the Siberian shelves, Canadian Arctic Archipelago and part of the Beaufort Sea affected by the McKenzie River. The surface of the Beaufort gyre becomes undersaturated before 2020, followed by widespread undersaturated conditions in the central Arctic before 2040. Areas affected by the Atlantic inflow become undersaturated last, during the 2080s.

In the case of calcite, undersaturation in the surface occurs 20–30 yr later than that of aragonite, and follows the same spatial progression (Fig. 5a, c). Siberian shelves become undersaturated first, starting from the inner shelves of the Kara and Laptev Seas and Canadian Arctic Archipelago, followed by the central Arctic Ocean. Areas affected by the Atlantic inflow (Greenland, Norwegian and Barents seas) do not show undersaturation within the 21st century. Shelf bottom water shows a similar timing of calcite undersaturation, except for the East Siberian Sea where undersaturation at the bottom occurs nearly two decades earlier than at the surface.

3.3 The Arctic from a global perspective

In this section we aim to compare the conditions influencing acidification and saturation state in the Arctic Ocean with those of the rest of the world ocean. One of the most important consequences of global warming for the marine biota and the ocean carbon system is the stabilisation of ocean stratification, leading to a reduction in the surface concentration of nutrients available for the net primary production as well as a stronger separation between surface layers in contact with the atmosphere from the intermediate and deep layers which have higher CT and lower (at the present day) Ω and pH_{SWS}. Globally averaged values of the maximum depth of mixing (Fig. 1d) show a shallowing of this depth from 137 to 127 m by the end of the century, although geographical variations are substantial (Fig. 6a, b). The most pronounced stabilisation of stratification

BGD
10, 2937–2965, 2013

occurs in the Pacific and Atlantic sectors of the Southern Ocean and in the northern North Atlantic, as well as in areas of the Atlantic inflow into the Arctic Ocean (Fig. 6b). The Arctic Ocean provides a marked exception from the general tendency of the ocean to stratify in response to climate warming. In the Arctic Ocean, stratification weakens with the exception of areas most affected by Atlantic inflow (see details in Sect. 3.1). This weakening of stratification tends to buffer the decline in pH_{SWS} and Ω caused by rising atmospheric CO_2.

In order to assess effects associated with nutrient regime, we chose to examine the variation in annual maximum of dissolved inorganic nitrogen (DIN). The stabilisation of stratification leads to a decline in globally averaged maximum surface DIN (Fig. 1c, d) although spatial patterns of its distribution show substantial geographical variation. While the majority of the surface ocean shows a decline of DIN (Fig. 6c, d), one notable exception is the northern North Pacific where weakening of the stratification allows access to subsurface waters rich in nutrients. The Arctic Ocean shows a strong decline in maximum DIN and widespread oligotrophic conditions in spite of the weakening of stratification, with the exception of areas affected by Pacific inflow which is characterised by relatively high DIN concentrations. Predicted global net primary production shows a consistent decline from 2010, falling by 6 % across the 21st century. The regional response of the net primary production, however, shows both positive and negative deviations after year 2000 (Fig. 6e, f). The two most prominent areas in this respect are the North Atlantic and the Arctic Ocean. In the former, the net primary production declines as a result of the shallowing of winter mixing. However, in the case of the latter, the net primary production increases over a substantial part of the basin as a result of the improved light regime (caused by sea-ice retreat) and higher nutrient supply rates (caused by weakening of stratification).

Increasing atmospheric CO_2 leads to an increase in surface CT (Fig. 7a–c), seen most prominently in the central Arctic Ocean. Globally, climate change effects mitigate this increase (Fig. 7c). This is most pronounced in the Northern North Atlantic and areas of the Arctic Ocean affected by inflows from the North Atlantic and Pacific. The

BGD
10, 2937–2965, 2013

impact of climate change is more substantial than that of the increase in CT in these areas due to the equilibration of the surface ocean with increasing atmospheric CO_2. The main mitigating factors in areas such as Arctic Ocean are the stabilisation of stratification (Fig. 6b) and the increase in the net primary production (Fig. 6f). However, the central Arctic Ocean is a pronounced exception, since here climate change accelerates the increase of surface CT due to the retreat of sea-ice (Sect. 4).

Following the increases in atmospheric and oceanic CO_2, globally averaged pH_{SWS} declines from 8.1 to 7.7 (Fig. 7d–f), this change being nearly homogeneous across the globe. Again, the Arctic Ocean is an exception, and here the basin-averaged pH_{SWS} decline is largest (−0.5), although there is strong spatial variability in this decline, ranging from −0.3 in the Greenland Sea to −0.6 in the Canada Basin (Fig. 4d). Climate change has only a small effect on pH_{SWS} because of the compensating temperature effect that buffers CT (e.g. McNeil and Matear, 2007). Once again, the Arctic Ocean is a special case where climate change factors (sea-ice retreat and surface freshening) accelerate the decline of pH_{SWS}, most noticeably in the central basin. While at present the Arctic Ocean is an area that exhibits some of the highest surface pH_{SWS} values in the World Ocean, it is predicted to become an area of the lowest pH_{SWS} by the end of the century as a result of climate change (Fig. 7d, e).

Ω_c and Ω_a are predicted to decline by 2 units globally (Fig. 1i). The decline is higher at low latitudes and lower at high latitudes, especially in the Arctic Ocean (Fig. 7i, l). On average, climate change mitigates the decrease of Ω, with maximum impact at high latitudes. Predicted changes in surface Ω by the end of the century are much less homogeneous than pH_{SWS} although, as for pH_{SWS}, the decline is maximal in the Arctic Ocean. Unlike pH_{SWS}, however, climate effects buffer changes in Ω brought about by the increased atmospheric CO_2 in nearly all ocean regions with the exception of most areas of the Arctic. In these latter areas, climate change effects accelerate the decline of Ω (Fig. 7i, l).

BGD
10, 2937–2965, 2013

4 Discussion

Due to polar amplification, the effect of climate change is greater at the poles compared to the rest of the globe. This amplification is thought to be largely a result of the retreat of sea-ice and associated feedbacks (e.g. Moritz et al., 2002). It is likely to continue in future, with the possibility of a seasonally ice-free Arctic in the 21st century (e.g. Zhang and Walsh, 2006). The ongoing retreat of sea-ice additionally brings about substantial changes to the freshwater balance of the region and increases the exposure of the ocean surface to the atmosphere with associated changes in ocean stratification and the net primary production. This increase in the spatial extent of open water in the Arctic Ocean also permits the equilibration of ocean and atmospheric CO_2 in areas previously covered by perennial ice, with resulting consequences for the associated carbonate chemistry. The Arctic Ocean has shown an early onset of the effects of acidification, characterised by low values of pH_{SWS} and carbonate saturation state (Yamamoto-Kawai et al., 2009). Observations already show undersaturated waters in various regions of the Arctic including the Canada Basin (Yamamoto-Kawai et al., 2009), freshwater-influenced shelves (Chierici and Fransson, 2009) and the Chukchi, Beaufort and eastern East Siberian Seas (Bates et al., 2011). A number of future projections for pH_{SWS} and Ω have been made using models that take into account the effects of climate change feedbacks (Orr et al., 2005; McNeil and Matear, 2007; Yamamoto et al., 2012). These studies have identified temperature, and its buffering effect on CO_2 exchange with the atmosphere, as the main climate change factor affecting undersaturation with respect to calcite and aragonite in the global ocean. The general consensus obtained in these studies is that climate change effects have little net impact on projected pH_{SWS} but that they substantially buffer the decline in Ω caused by increasing CO_2. The Arctic Ocean however, is a considerably more complex region. Melting sea-ice causes pH_{SWS} and Ω to decline markedly (McNeil and Matear, 2007; Yamamoto et al., 2012), both as a result of the relatively low pH_{SWS} of melting ice water and because of the greater exposure of previously ice-covered waters to the

BGD
10, 2937–2965, 2013

atmosphere and the consequent ventilation of CO_2. Various projections show that the Arctic Ocean will become locally understaurated (in at least one month per year) with respect to aragonite within the current decade (2010–2020) and with respect to calcite during the decade 2040–2050 (McNeil and Matear, 2007; Steinacher et al., 2009; Yamamoto et al., 2012).

Our results are in general agreement with the previous projections described above. They indicate that the Arctic is the first ocean basin to exhibit widespread undersaturation (Fig. 8b, d). We have focused our examination on the strong spatial gradients seen in physical and biogeochemical properties of the Arctic Ocean, which have important consequences for the time evolution of pH_{SWS} and carbonate saturation state. The impact of the various climate change drivers on ocean acidification and saturation state in the Arctic is a complex problem to address when making future projections. The various drivers include: (i) increase in the temperature of seawater, which directly affects carbonate chemistry and biological production, as well as indirectly affecting the same characteristics via changes in ocean stratification; (ii) changes in the freshwater balance and energy exchange with the atmosphere affecting ocean stratification, which regulate not only the atmospheric exchange of CO_2 but also the mixing of deep waters – which are characterised by higher nutrient and lower (at present day) pH_{SWS} and Ω – to the surface; (iii) retreat of sea-ice, which accelerates uptake of atmospheric CO_2 by the ocean, as well as influencing stratification and providing freshwater inputs that lower pH_{SWS} and Ω; (iv) increase in riverine input, lowering pH_{SWS} and Ω and also stabilising ocean stratification.

The various climate-related factors were predicted by our model to operate differently in the various regions of the Arctic Ocean, their role varying from acceleration of acidification rates through to a strong buffering effect. The Canadian Arctic Archipelago and Baffin Bay have the highest inputs of freshwater from melting sea-ice which, because of its relative acidity, causes pH_{SWS} and Ω to decline. These regions bear the brunt of the transition towards a seasonally ice-free state as the sea-ice retreats, with the result that they experience greater ventilation of CO_2 with the atmosphere which

BGD
10, 2937–2965, 2013

in turn further decreases pH_{SWS} and saturation state. The Siberian shelves, in contrast, show little response to climate change in terms of pH_{SWS} and saturation state because increased fresh water input is largely compensated for by elevated rates of the net primary production. A further variation in climate change impacts is seen in areas affected by the Atlantic inflow, namely the Greenland Sea and outer shelves of the Barents, Kara and Laptev seas. In these regions, weakening stratification associated with diminishing sea-ice cover leads to increased net primary production as nutrient rich waters are mixed in from below. Decreases in pH_{SWS} and saturation state are therefore minimised, both because of decreasing CT levels at the surface due to the net primary production and because CO_2 invading the ocean is effectively diluted over a greater depth range.

The results from our model indicate that timing of the onset of undersaturation is highly variable across the Arctic, occurring during the decade of 2000–2010 in the Siberian shelves and Canadian Arctic Archipelago, but as late as the 2080s for the Barents and Norwegian Seas (corresponding to atmospheric pCO_2 of 350–400 ppm and 750–800 ppm, respectively: Figs. 5b and 8c).

The future projections presented herein are based on the RCP 8.5 scenario which ostensibly represents an upper bound of anthropogenic carbon emissions currently under consideration for the upcoming IPCC Fifth Assessment Report. However, as things stand today, observed emissions are already reaching this level (e.g. Peters et al., 2012), suggesting the possibility that future emissions, and associated atmospheric CO_2, could be even higher. In the event that future emissions are higher than the RCP 8.5 scenario, undersaturation will occur even faster than indicated by our model results. The atmospheric CO_2 levels that correspond to the onset of aragonite undersaturation, and how this varies spatially within the Arctic Ocean, are shown in Fig. 8. As a first approximation, the CO_2 levels shown in this figure may be considered independent of any particular emission scenario. This analysis indicates that widespread Arctic Ocean undersaturation with respect to aragonite occurs before atmospheric CO_2 reaches 500 ppm. In contrast, the Southern Ocean only begins to

BGD
10, 2937–2965, 2013

experience widespread undersaturation in surface waters when atmospheric CO_2 exceeds 550 ppm (year 2050 under RCP 8.5).

We conclude that, in order to make future projections of acidification and carbon saturation state in the Arctic, models of sufficiently high resolution are needed to address regional aspects of physical and biological dynamics. The use of basin-averaged characteristics, while useful for model intercomparison studies, is not optimal for predicting, for example, the timing of the first occurrence of aragonite undersaturation in the Arctic. Forecasting the future progression of ocean acidification in the Arctic Ocean is challenging given the complexity of ocean-atmosphere feedbacks, especially the role of retreating sea-ice, as well as being hampered by the paucity observations available for model verification. A major source of uncertainty in future projections of ocean acidification in the Arctic Ocean is the difference in the sea-ice reduction rates projected by climate models (Yamamoto et al., 2012). Our results confirm this conclusion and stress the need for careful model intercomparison studies of Arctic Ocean acidification, with a particular focus on differences in the modelled decline of sea-ice.

5 Conclusions

- We compared two runs of a global ocean general circulation model that includes biogeochemistry and the carbon cycle, forced by the RCP 8.5 emission scenario and run to year 2099. We separated the impacts of rising atmospheric CO_2 from associated future climate change and showed that climate change feedbacks play a strong role in the Arctic Ocean driving spatial heterogeneity of declines in Ω and pH_{SWS} in this basin.
- Simulation results indicate that the Arctic is the first ocean basin to exhibit widespread surface undersaturation with respect to aragonite and, later, calcite. The onset of surface undersaturation shows great variability between different regions of the Arctic Ocean as a result of differences in climate change feedback

BGD
10, 2937–2965, 2013

factors such as the retreat of sea-ice, changes in freshwater input and changes in stratification. The timing of the first occurrence of surface undersaturation with respect to aragonite varies across the Arctic Ocean by nearly a century. Our results thus caution against using coarse resolution models when modelling future changes in acidification and saturation state in the Arctic.

– In line with the previous studies (e.g. Yamamoto et al., 2012), the strongest driving force and the largest uncertainty in prediction of acidification in the Arctic and its response to changing climate is the rate of decline of sea-ice. Model intercomparison studies that address acidification rates in the Arctic Ocean need to assess the associated processes in relation to model projections of sea-ice retreat.

Acknowledgements. The authors acknowledge the financial support of the Natural Environmental Research Council (NERC) within the framework of National Capability and NERC UK Ocean Acidification research programme (Regional Ocean Modelling project). The authors are additionally grateful to the NEMO development team at NOC for their technical support throughout this work. In particular, the assistance of Beverly de Cuevas and Steven Alderson has been invaluable in the development and simulation of MEDUSA-2. The HadGEM2-ES atmospheric forcing was produced by the UKMO and made available for use by NEMO by Dan Bernie (UKMO). The carbonate chemistry scheme utilised by MEDUSA-2 to calculate, among other things, air–sea CO_2 flux was generously supplied by Jerry Blackford (PML). The benthic reservoir scheme used here is based on a similar scheme developed, and supplied, by Momme Butenschon (PML). We would like to acknowledge a substantial role of AOMIP/FAMOS as an excellent forum for exchange of ideas in all aspects of Arctic Ocean modelling and observations.

Edited by: A. Nonymous

BGD
10, 2937–2965, 2013

References

Anderson, T. R.: Plankton functional type modelling: running before we can walk? J. Plankton Res., 27, 1073–1081, doi:10.1093/plankt/fbi076, 2005.

Bates, N. R., Cai, W.-J., and Mathis, J. T.: The ocean carbon cycle in the western Arctic Ocean distributions and air-sea fluxes of carbon dioxide, Oceanography, 24, 186–201, doi:10.5670/oceanog.2011.71, 2011. 2940, 2949

Bates, N. R., Orchowska, M. I., Garley, R., and Mathis, J. T.: Seasonal calcium carbonate undersaturation in shelf waters of the Western Arctic Ocean; how biological processes exacerbate the impact of ocean acidification, Biogeosciences Discuss., 9, 14255-14290, doi:10.5194/bgd-9-14255-2012, 2012. 2942

Carmack, E. and Wassmann, P.: Food webs and physical-biological coupling on pan-Arctic shelves: Unifying concepts and comprehensive perspectives, Prog. Oceanogr., 71, 446–477, doi:10.1016/j.pocean.2006.10.004, 2006.

Carmack, E., D. Barber, J. Christensen, R. Macdonald, B. Rudels, and E. Sakshaug: Climate variability and physical forcing of the food webs and the carbon budget on panarctic shelves, Prog. Oceanogr., 71, 145–181, doi:10.1016/j.pocean.2006.10.005, 2006. 2940

Chierici, M. and Fransson, A.: Calcium carbonate saturation in the surface water of the Arctic Ocean: undersaturation in freshwater influenced shelves, Biogeosciences, 6, 2421–2431, doi:10.5194/bg-6-2421-2009, 2009. 2940, 2942, 2949

Collins, W. J., Bellouin, N., Doutriaux-Boucher, M., Gedney, N., Halloran, P., Hinton, T., Hughes, J., Jones, C. D., Joshi, M., Liddicoat, S., Martin, G., O'Connor, F., Rae, J., Senior, C., Sitch, S., Totterdell, I., Wiltshire, A., and Woodward, S.: Development and evaluation of an Earth-System model – HadGEM2, Geosci. Model Dev., 4, 1051–1075, doi:10.5194/gmd-4-1051-2011, 2011. 2941

Fabry, V. J., Seibel, B. A., Feely, R. A., and Orr, J. C.: Impacts of ocean acidification on marine fauna and ecosystem processes, ICES J. Mar. Sci., 65, 414–432, doi:10.1093/icesjms/fsn048, 2008. 2939

Friedlingstein, P., Houghton, R. A., Marland, G., Hackler, J., Boden, T. A., Conway, T. J., Canadell, J. G., Raupach, M. R., Ciais, P., and Le Quéré, C.: Update on CO_2 emissions, Nat. Geosci., 3, 811–812, doi:10.1038/ngeo1022, 2010. 2939

Gangstø, R., Joos, F., and Gehlen, M.: Sensitivity of pelagic calcification to ocean acidification, Biogeosciences, 8, 433-458, doi:10.5194/bg-8-433-2011, 2011. 2939

BGD
10, 2937–2965, 2013

Gaspar, P., Grégoris, Y., and Lefevre, J.-M.: A simple eddy kinetic energy model for simulations of the oceanic vertical mixing Tests at station papa and long–term upper ocean study site, J. Geophys. Res., 95, 16179–16193, 1990. 2941

Gruber, N.: Warming up, turning sour, losing breath: ocean biogeochemistry under global change, Philos. T. R. Soc. A, 369, doi:10.1098/rsta.2011.0003, 2011.

Houghton, J. T., Ding, Y., Griggs, D. J., Noguer, M., van der Linden, P. J., Dai, X., Maskell, K., and Johnson, C. A. (Eds.): Intergovernmental Panel on Climate Change 2001: the scientific basis, Cambridge University Press, Cambridge, UK, 881 pp., 2001. 2939

Jones, C. D., Hughes, J. K., Bellouin, N., Hardiman, S. C., Jones, G. S., Knight, J., Liddicoat, S., O'Connor, F. M., Andres, R. J., Bell, C., Boo, K.-O., Bozzo, A., Butchart, N., Cadule, P., Corbin, K. D., Doutriaux-Boucher, M., Friedlingstein, P., Gornall, J., Gray, L., Halloran, P. R., Hurtt, G., Ingram, W. J., Lamarque, J.-F., Law, R. M., Meinshausen, M., Osprey, S., Palin, E. J., Parsons Chini, L., Raddatz, T., Sanderson, M. G., Sellar, A. A., Schurer, A., Valdes, P., Wood, N., Woodward, S., Yoshioka, M., and Zerroukat, M.: The HadGEM2-ES implementation of CMIP5 centennial simulations, Geosci. Model Dev., 4, 543–570, doi:10.5194/gmd-4-543-2011, 2011. 2941

Jutterström, S. and Anderson, L. G.: The saturation of calcite and aragonite in the Arctic Ocean, Mar. Chem., 94, 101–110, doi:10.1016/j.marchem.2004.08.010, 2005. 2942

Khatiwala, S., Primeau, F., and Hall, T.: Reconstruction of the history of anthropogenic CO_2 concentrations in the ocean, Nature, 462, 346-U110, doi:10.1038/nature08526, 2009. 2939

Madec, G.: NEMO reference manual, ocean dynamic component: NEMO–OPA, Note du Pole de modélisation, Institut Pierre Simon Laplace, Technical Report 27, Note du pôle de modélisation, Institut Pierre Simmon Laplace, France, No. 27, ISSN No. 1288–1619, 2008. 2941

McNeil, B. I. and Matear, R. J.: Climate change feedbacks on future oceanic acidification, Tellus B, 59, doi:10.1111/j.1600-0889.2006.00241.x, 2007. 2939, 2940, 2943, 2948, 2949, 2950

Moritz, R. E., Bitz, C. M., and Steig, E. J.: Dynamics of recent climate change in the Arctic, Science, 297, 1497–1502, doi:10.1126/science.1076522, 2002. 2939, 2943, 2949

Orr, J. C., Fabry, V. J., Aumont, O., Bopp, L., Doney, S. C., Feely, R. A., Gnanadesikan, A., Gruber, N., Ishida, A., Joos, F., Key, R. M., Lindsay, K., Maier-Reimer, E., Matear, R., Monfray, P., Mouchet A., Najjar, R. G., Plattner, G. K., Rodgers, K. B., Sabine, C. L., Sarmiento, J. L., Schlitzer, R., Slater, R. D., Totterdell, I. J., Weirig, M. F., Yamanaka, Y., and Yool, A.:

BGD
10, 2937–2965, 2013

Anthropogenic ocean acidification over the twenty-first century and its impact on calcifying organisms, Nature, 437, 681–686, 2005. 2949

Pachauri, R. K. and Reisinger, A. (Eds.): Contribution of Working Groups I, II and III to the Fourth Assessment Report of the Intergovernmental Panel on Climate Change Core Writing Team, IPCC, Geneva, Switzerland, 104 pp., 2007.

Peters, G. P., Andrew, R. M., Boden, T., Canadell, J. G., Ciais, P., Le Quéré, C., Marland, G., Raupach, M. R., Wilson, C.: The challenge to keep global warming below 2 °C, Nature Clim. Change, doi:10.1038/nclimate1783, 2012. 2951

Popova, E. E., Yool, A., Coward, A. C., Aksenov, Y. K., Alderson, S. G., de Cuevas, B. A., and Anderson, T. R.: Control of primary production in the Arctic by nutrients and light: insights from a high resolution ocean general circulation model, Biogeosciences, 7, 3569–3591, doi:10.5194/bg-7-3569-2010, 2010. 2940, 2942

Popova, E. E., Yool, A., Coward, A. C., Dupont, F., Deal, C., Elliott, S., Hunke, E., Jin, M., Steele, M., and Zhang, J.: What controls primary production in the Arctic Ocean? Results from an intercomparison of five general circulation models with biogeochemistry, J. Geophys. Res.-Oceans, 117, C00D12, doi:10.1029/2011JC007112, 2012. 2942

Ridgwell, A., Zondervan, I., Hargreaves, J. C., Bijma, J., and Lenton, T. M.: Assessing the potential long-term increase of oceanic fossil fuel CO_2 uptake due to CO_2-calcification feedback, Biogeosciences, 4, 481–492, doi:10.5194/bg-4-481-2007, 2007.

Sabine, C. L., Feely, R. A., Gruber, N., Key, R. M., Lee, K. J., Bullister, L., Wanninkhof, R., Wong, C. S., Wallace, D. W. R., Tilbrook, B., Millero, F. J., Peng, T. H., Kozyr, A., Ono, T., and Rios, A. F.: The oceanic sink for anthropogenic CO_2, Science, 305, 367–371, doi:10.1126/science.1097403, 2004. 2939

Steinacher, M., Joos, F., Frölicher, T. L., Plattner, G.-K., and Doney, S. C.: Imminent ocean acidification in the Arctic projected with the NCAR global coupled carbon cycle-climate model, Biogeosciences, 6, 515–533, doi:10.5194/bg-6-515-2009, 2009. 2940, 2950

Stroeve, J., Holland, M. M., Meier, W., Scambos, T., and Serreze, M.: Arctic sea ice decline: Faster than forecast, Geophys. Res. Lett., 34, L09501, doi:10.1029/2007GL029703, 2007.

Timmermann, R., Goosse, H., Madec, G., Fichefet, T., Ethe, C., and Duliere, V.: On the representation of high latitude processes in the ORCA-LIM global coupled sea ice-ocean model, Ocean Model, 8, 175–201, doi:10.1016/j.ocemod.2003.12.009, 2005. 2941

Walsh, J. E., Overland, J. E., Groisman, P. Y., and Rudolf, B.: Ongoing climate change in the Arctic, Ambio, 40, 6–16, doi:10.1007/s13280-011-0211-z, 2011. 2939

BGD
10, 2937–2965, 2013

Yamamoto, A., Kawamiya, M., Ishida, A., Yamanaka, Y., and Watanabe, S.: Impact of rapid sea-ice reduction in the Arctic Ocean on the rate of ocean acidification, Biogeosciences, 9, 2365–2375, doi:10.5194/bg-9-2365-2012, 2012. 2940, 2949, 2950, 2952, 2953

Yamamoto-Kawai, M., McLaughlin, F. A., Carmack, E. C., Nishino, S., and Shimada, K.: Aragonite undersaturation in the Arctic Ocean: effects of ocean acidification and sea ice melt, Science, 326, doi:10.1126/science.1174190, 2009. 2940, 2949

Yool, A., Popova, E. E., and Anderson, T. R.: Medusa-1.0: a new intermediate complexity plankton ecosystem model for the global domain, Geosci. Model Dev., 4, 381–417, doi:10.5194/gmd-4-381-2011, 2011. 2942

Yool, A., Popova, E. E., and Anderson, T. R.: MEDUSA-2: An intermediate complexity biogeochemical model of the marine carbon cycle for climate change and ocean acidification studies, Geosci. Model Dev., submitted, 2013a. 2942

Yool, A., Popova, E. E., and Anderson, T. R.: Climate change and ocean acidification impacts on lower trophic levels and export of organic carbon to the deep ocean, Biogeosciences, in press, 2013b. 2941, 2942

Zhang, X. and Walsh, J. E.: Toward a seasonally ice-covered Arctic Ocean: Scenarios from the IPCC AR4 model simulations, J. Climate, 19, 1730–1747, doi:10.1175/JCLI3767.1, 2006. 2949

BGD
10, 2937–2965, 2013

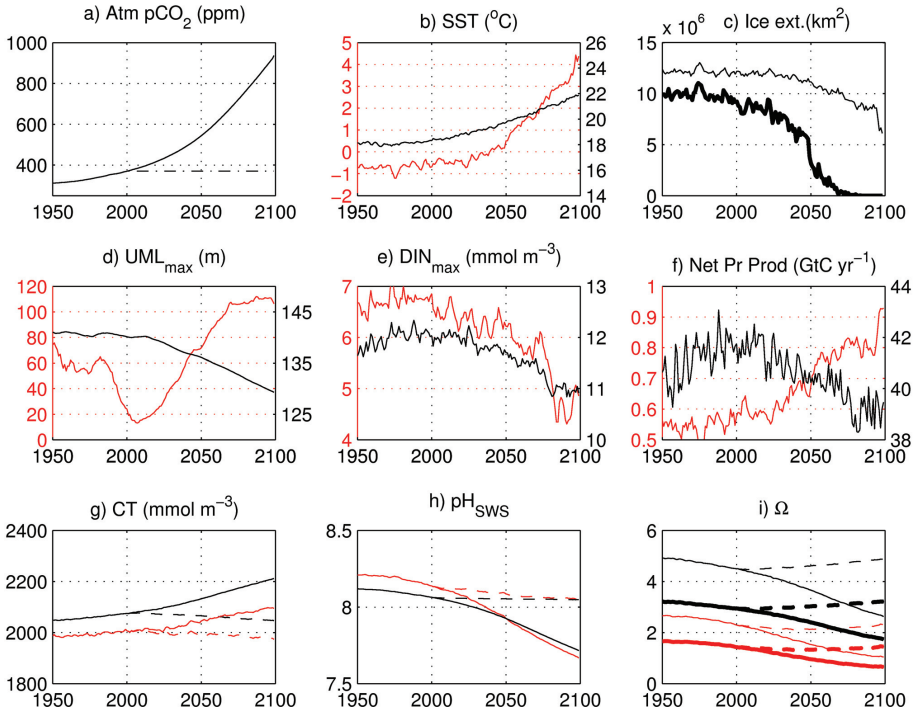

Fig. 1. Time evolution of modelled characteristics for the global ocean (black line and font) and the Arctic Ocean (treated as north of 66° N, red line and font): **(a)** atmospheric CO_2 (ppm); **(b)** sea surface temperature (°C); **(c)** volume of the Northern Hemisphere sea-ice (km^3); **(d)** maximum depth of the upper mixed layer UML, (m); **(e)** surface dissolved inorganic nitrogen (DIN, $mmol\,m^{-3}$); **(f)** water-column integrated net primary production ($gC\,m^{-2}\,yr^{-1}$); **(g)** surface CT ($mmol\,m^{-3}$); **(h)** pH_{SWS}; **(i)** Ω_c and Ω_a. Annual mean characteristics are given for all properties except for the ice volume **(c)** where monthly mean values are shown. For **(g–i)** dashed lines refer to the "climate-effect" run (no CO_2 increase), for **(i)** thin line refers to Ω_c, thick line refers to Ω_a.

BGD
10, 2937–2965, 2013

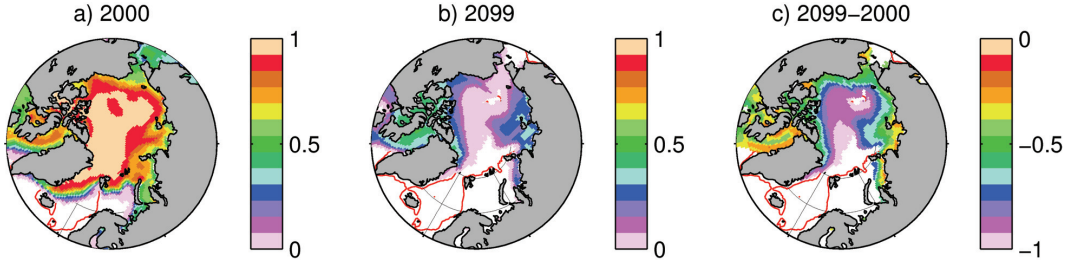

Fig. 2. Arctic Ocean annual mean ice concentration for year 2000 **(a)**, 2099 **(b)**, difference between year 2099 and 2000 **(c)**.

BGD
10, 2937–2965, 2013

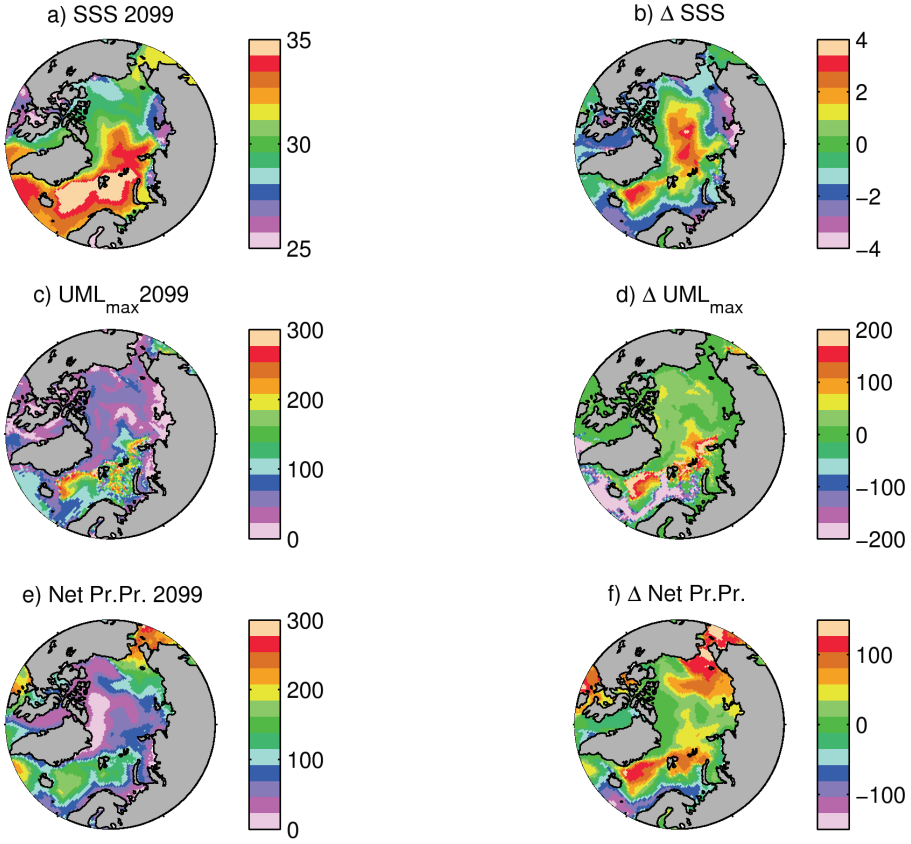

Fig. 3. Arctic Ocean surface salinity **(a, b)**, maximum upper mixed layer depth (UML, **(c, d)** in m, net primary production **(a–c)** in $g C m^{-2} yr^{-1}$. The first column shows values for year 2099, the second column shows deviation between year 2099 and year 2000.

BGD
10, 2937–2965, 2013

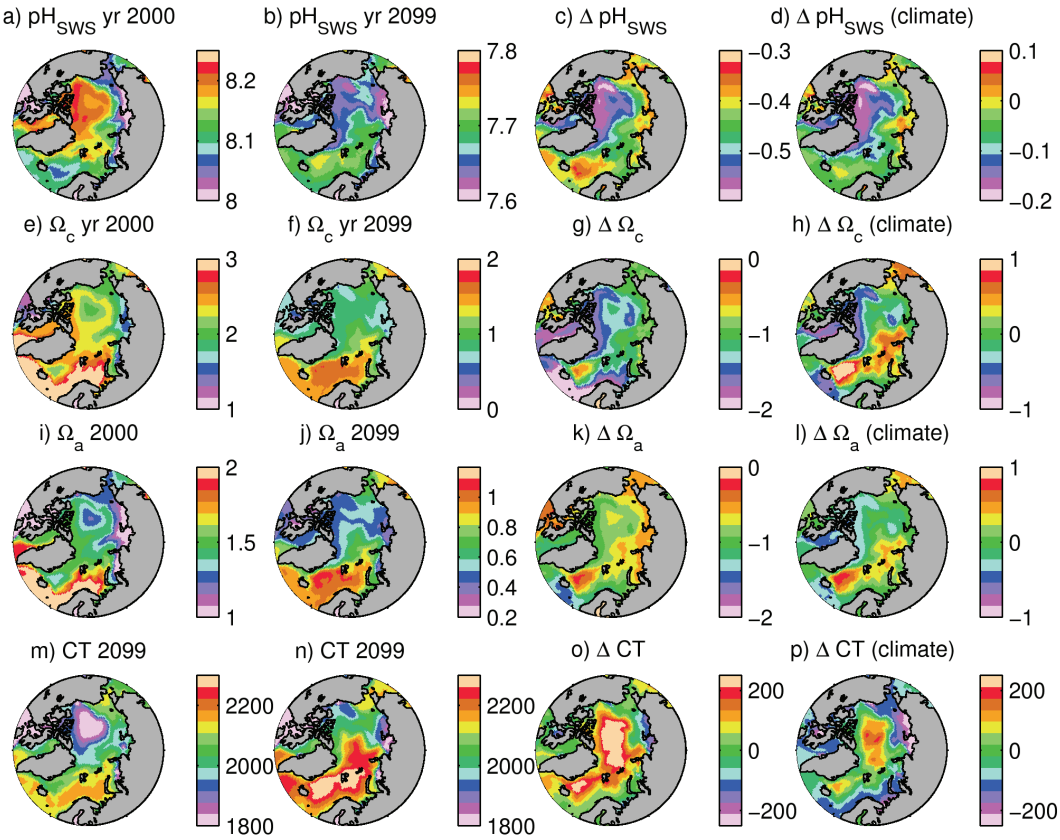

Fig. 4. Arctic Ocean pH$_{SWS}$ **(a–d)**, Ω$_c$ **(e–h)**, Ω$_a$ **(i–l)**, CT (mmol m^{-3}, **m–n**). The first and second columns shows values for year 2000 and 2099 respectively, the third column shows deviation between year 2099 and year 2000 for the full run, and the fourth column shows deviation between year 2099 and year 2000 for the for the climate change run.

BGD
10, 2937–2965, 2013

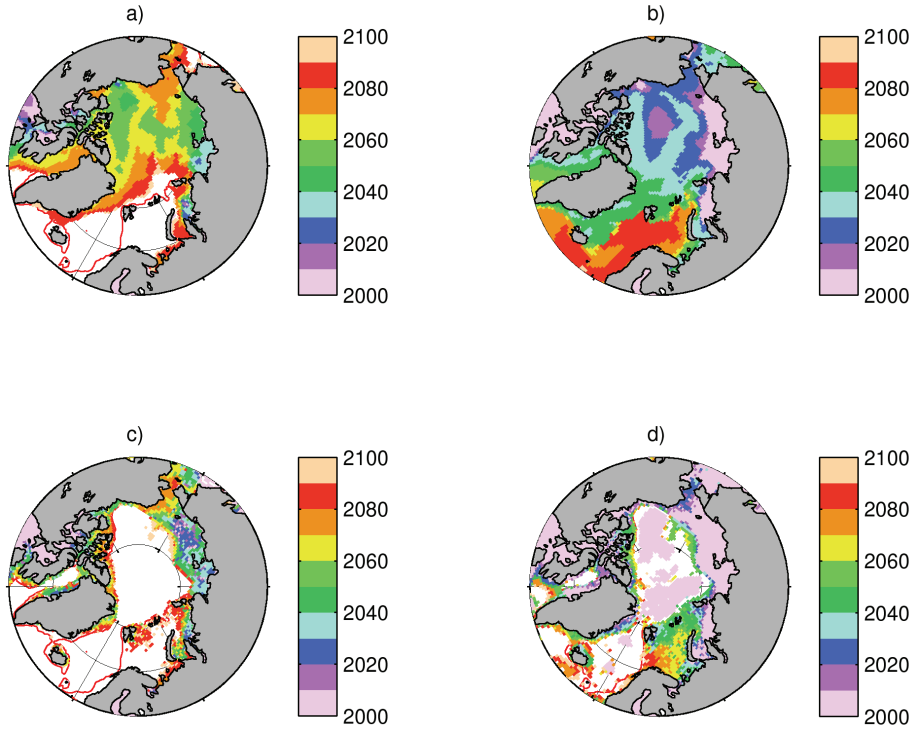

Fig. 5. The first occurrence of a monthly mean undersaturated surface waters in respect to calcite **(a)** and aragonite (**b**, years). The same for the bottom waters at the depth of the deepest model vertical grid box **(c, d)**.

BGD
10, 2937–2965, 2013

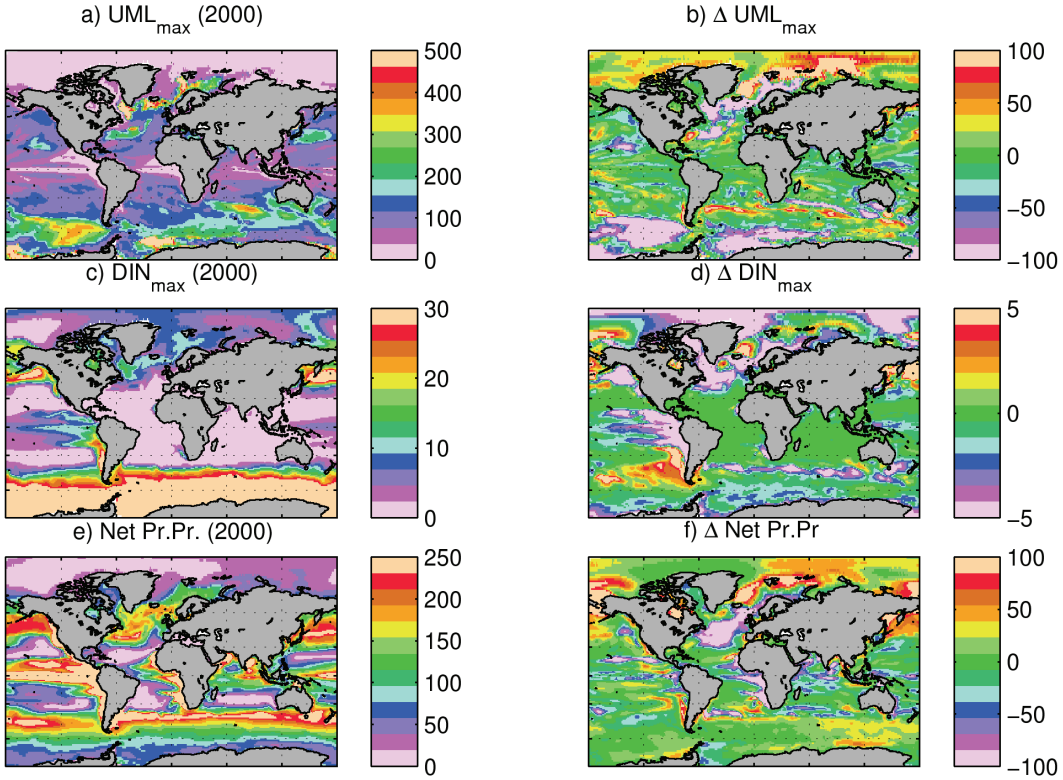

Fig. 6. Global surface maps of the upper mixed layer maximum (**a, b**, in m), surface DIN (**c, d** in mmol m^{-3}), net primary production (**e, f** in g C m^{-2} yr^{-1}). Values are given for year 2000 (left column) and for deviation between year 2099 and year 2000 (right column).

BGD
10, 2937–2965, 2013

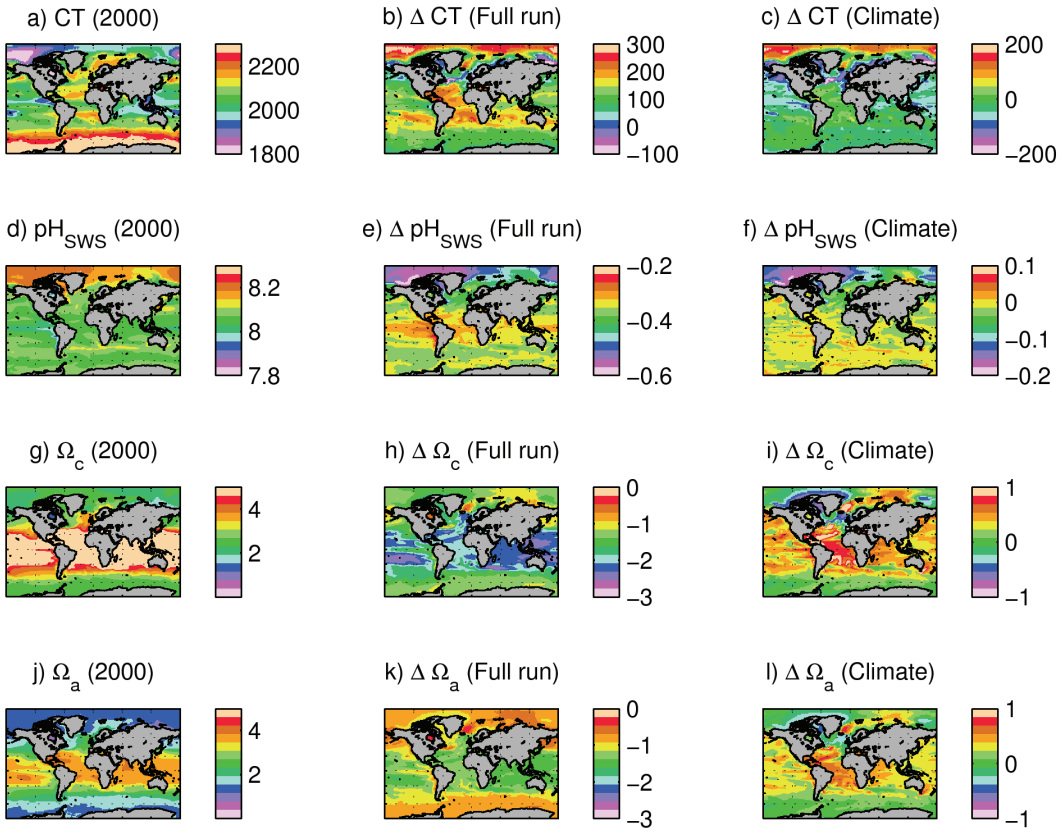

Fig. 7. Global surface maps of CT (mmol m^{-3}) **(a–c)**, pH$_{SWS}$ **(d–f)**, Ω_c **(g–h)** and Ω_a **(j–l)**. The first column shows values for year 2000; the second column shows deviation between year 2099 and year 2000 for the full run, and the third column shows deviation between year 2099 and year 2000 for the for the climate change run.

BGD
10, 2937–2965, 2013

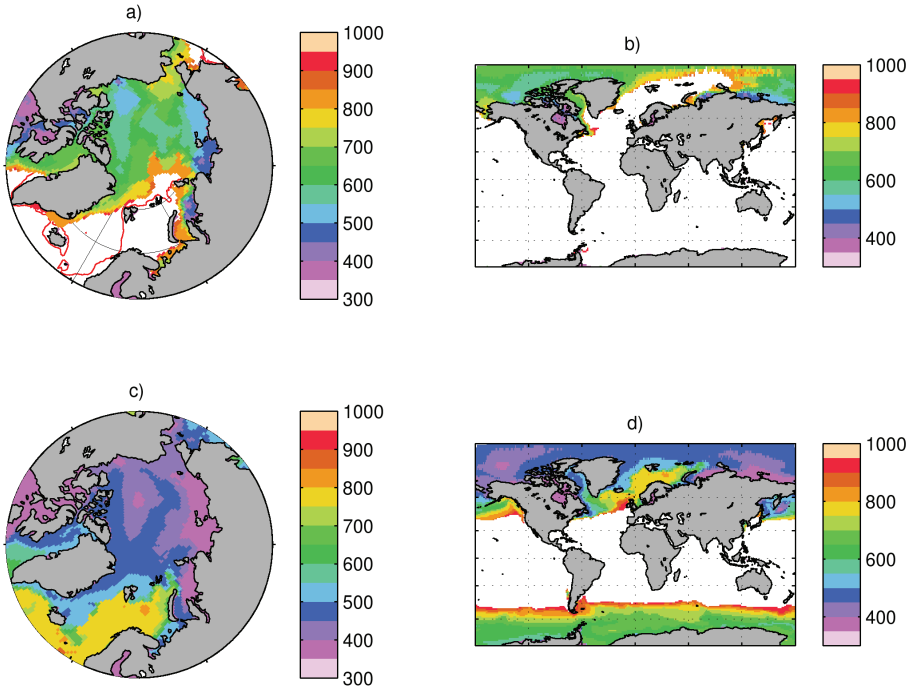

Fig. 8. Level of atmospheric CO_2 (ppm) under which monthly mean undersaturated surface waters occur fist time in respect to calcite **(a, b)** and aragonite **(c, d)**.

BGD
10, 2937–2965, 2013